JOURNAL OF MATERIALS SCIENCE **36** (2001) 3737–3744

Hydrothermal degradation mechanism of tetragonal Zirconia

XIN GUO
State Key Laboratory of Advanced Technology for Materials Synthesis and Processing, Wuhan, Hubei Province 430070, People's Republic of China; Department of Materials Science and Engineering, Huazhong University of Science and Technology, Wuhan, Hubei Province 430074, People's Republic of China
E-mail: guo@chemix.mpi-stuttgart.mpg.de

The hydrothermal degradation mechanism of tetragonal ZrO_2 previously proposed by the author was elaborated. In this mechanism, the annihilation of oxygen vacancies is a crucial step, and the grain boundaries play an important role in propagating the degradation. The degradation process of a 3 mol% Y_2O_3 doped ZrO_2 pellet annealed in water vapor was monitored via impedance spectroscopy, the bulk and the grain boundary resistivity, and the grain boundary thickness were all found to increase with increasing annealing time, proving the annihilation of oxygen vacancies in the bulk and especially at the grain boundaries. The fracture surfaces of the annealed pellet were studied by SEM, only intergranular cracks were observed, indicating the propagation of the degradation along the grain boundaries. The mechanism predicts that the electrode resistance should increase when the electrodes are exposed to water vapor. Silver electrodes on a 8 mol% Y_2O_3 doped ZrO_2 pellet were annealed in the mixture of oxygen and water vapor, the electrode resistance was found to increase with increasing annealing time. The prediction was thus proven.

1. Introduction

Tetragonal ZrO_2 was found to undergo an unusual spontaneous tetragonal to monoclinic transformation with the presence of water vapor when annealed at relatively low temperatures (65 to 400 °C) [1–19], engendering cracks in the transformed surface due to the volume expansion accompanying the phase transformation, thereby severely degrading the mechanical properties. This phenomenon is called "(low temperature) hydrothermal degradation of tetragonal ZrO_2".

Much research has been performed on the degradation, the following features have been established: (1) the tetragonal to monoclinic transformation proceeds from the surface to the interior [1–19]; (2) of all the major constituents of air, only water vapor causes the tetragonal to monoclinic transformation [4–10], and the degradation is greatly accelerated by the presence of water [12–17]; (3) the degradation is marked only for ZrO_2 ceramics with low dopant content [3, 10, 11], (4) grain size has a significant effect on the degradation, both decreasing [3, 4, 10, 11] and increasing [12] grain size can retard the degradation.

Many attempts have been taken to explain the degradation, some typical mechanisms can be summarized as follows: Lange *et al*. [10] observed $Y(OH)_3$ crystallites in the degraded ZrO_2-Y_2O_3 ceramics, therefore, they suggested that water vapor reacted with Y_2O_3 to form the crystallites, the reaction locally drew Y_2O_3 from tetragonal grains, transforming the tetragonal grains to monoclinic ones; on the other hand, Sato *et al*. [4] proposed that water vapor reacted with Zr-O-Zr bonds and Zr-OH bonds were formed; however, according to Yoshimura *et al*. [13, 14] the dissociation of H_2O at the ZrO_2 surface and the formation of Zr-OH or Y-OH bonds, resulting in the lattice strain at the surface, promoted the tetragonal to monoclinic transformation; Hernandez *et al*. [15] proposed that the reaction of OH^- ions in the more active points (Y_2O_3) to form an oxyhydroxide YO(OH) species was the key process responsible for the degradation of Y_2O_3-stabilized ZrO_2.

The mechanisms proposed by Sato *et al*. [4] and Yoshimura *et al*. [13, 14] cannot explain the effects of grain size and dopant level. While the mechanisms proposed by Lange *et al*. [10] and Hernandez *et al*. [15] can explain the effect of dopant level, but they cannot explain the effect of grain size either.

Recently, the degradation has been re-studied by the author [20–23] with X-ray photoelectron spectroscopy (XPS). OH^- ions were observed on the ZrO_2 surfaces by XPS (see Fig. 1), suggesting the dissociation of H_2O on the surfaces. A plausible way of forming an OH^- ion is that an adsorbed water molecule H_2O reacts with an oxygen on the surface O''_{surf} which may come from the lattice oxygen resulting from the termination of the periodical ZrO_2 lattice at the surface and/or adsorbed oxygen from the air

$$H_2O_{ad} + O''_{surf} \rightarrow 2(OH)'_{surf} \quad (1)$$

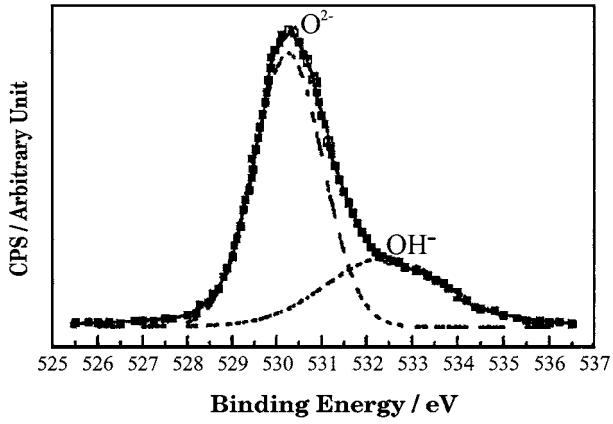

Figure 1 O1s XPS spectrum of the surface of 3 mol% Y_2O_3 doped ZrO_2 after annealing in boiling water for 40 h [20] (solid squares: experimental points, dotted lines: peak-fitting results). The fitting peak at the lower binding energy is characteristic of O^{2-} ions, while the one at the higher binding energy is typical of OH^- ions. Therefore, OH^- ions were formed on the ZrO_2 surface during annealing.

where $(OH)'_{surf}$ is an OH^- ion on the ZrO_2 surface. Doping (usually with Y_2O_3, CaO or MgO) introduces large numbers of oxygen vacancies $V_O^{\bullet\bullet}$ into the ZrO_2 lattice. By the diffusion of $V_O^{\bullet\bullet}$ and/or $(OH)'_{surf}$, a further defect reaction may occur as follows

$$(OH)'_{surf} + V_O^{\bullet\bullet} \rightarrow (OH)_O^{\bullet} + S^x_{O,surf} \qquad (2)$$

where $(OH)_O^{\bullet}$ is an OH^- ion on the oxygen site in the ZrO_2 lattice, $S^x_{O,surf}$ is a vacant surface site for oxygen.

Higher OH^- concentration at the grain boundaries of a sample annealed in boiling water for 40 h was also detected by XPS (see Fig. 2), suggesting the occurrence of the grain boundary diffusion of the OH^- ions. The

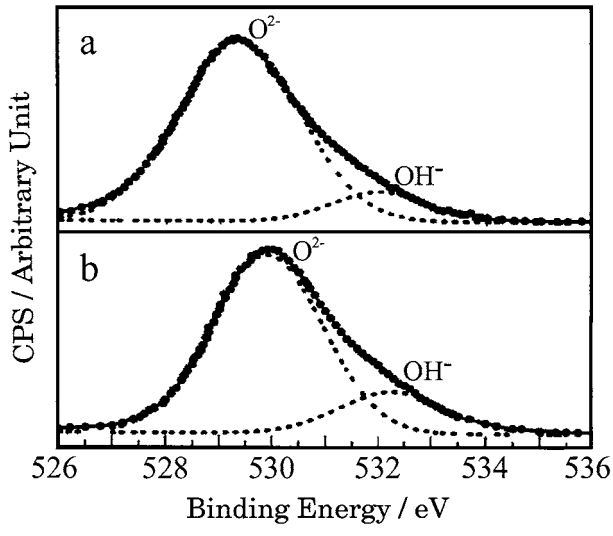

Figure 2 O1s XPS spectra of the grain boundaries of 3 mol% Y_2O_3 doped ZrO_2 after annealing in boiling water for 40 h: (a) before annealing, (b) after annealing [21] (solid circless: experimental points, dotted lines: peak-fitting results). The XPS analyses were performed on the fracture suefaces, because the fracture is inter-granular. As the number of O^{2-} ions should remain almost unchanged after annealing, we can use the area ratio of the peak OH^- to the peak O^{2-} as an estimate of the number of the OH^- ions. After annealing, the area ratio increased from about 0.13 to about 0.23, suggesting that some OH^- ions intergranularly diffused into the interior of the sample during annealing.

OH^- ions at the grain boundaries may also react with the oxygen vacancies there, in this case, the reaction should be written as

$$(OH)'_{gb} + V_O^{\bullet\bullet} \rightarrow (OH)_O^{\bullet} + S^x_{O,gb} \qquad (3)$$

where $(OH)'_{gb}$ is an OH^- ion at the grain boundaries, $S^x_{O,gb}$ is a vacant grain-boundary site for oxygen.

Livage *et al.* [24] suggested that oxygen vacancies play an important role in the stabilization of ZrO_2. By creating and annihilating oxygen vacancies in ZrO_2, Kountouros and Petzow [25] proved that there are a critical minimum and a critical maximum oxygen-vacancy concentration for the cubic, the tetragonal and the monoclinic phase, respectively, sufficient oxygen-vacancy concentration variation will result in phase transformation.

By reaction (2), the oxygen vacancies in the surface layers are annihilated, when the oxygen-vacancy concentration is reduced to such an extent that a tetragonal to monoclinic transformation takes place in the surface layers. If the amount of the phase transformation is large enough, due to the volume expansion associated with the phase transformation, both micro- and macro-cracks can be produced in the transformed surface layers, and the cracks open up new surfaces to react with water or water vapor, leading to a further spontaneous transformation. By reaction (3), the oxygen vacancies at the grain boundaries are also annihilated.

Therefore, a new mechanism was proposed [20–23]: (1) chemical adsorption of H_2O on ZrO_2 surface, (2) reaction of H_2O with O^{2-} on the ZrO_2 surface to form OH^- ions, (3) penetration of OH^- ions into the inner part by grain-boundary diffusion, (4) annihilation of oxygen vacancies by OH^- ions, (5) when the oxygen-vacancy concentration is reduced so that the tetragonal phase is no longer stable, a tetragonal to monoclinic transformation occurrs, further degradation can expand along the grain boundaries and the cracks.

This new mechanism requires only diffusions of oxygen vacancies and/or OH^- ions, the rates of which are still high enough at low temperatures, especially that of OH^- ions [26]. Both increasing dopant content and decreasing grain size can increase the oxygen vacancy concentration in the surfaces and at the grain boundaries [20, 21, 27], also in the bulk in the case of increasing dopant content, thus more vacancies should be annihilated to induce the degradation. The grain boundaries play an important role in propagating the degradation, increasing grain size decreases the grain boundary area, thus retarding the degradation [21]. Owing to its comparatively large grain size, relatively high oxygen vacancy concentration and very thin vacancy depletion layers in the surfaces and at the grain boundaries, such a degradation never occurrs for cubic ZrO_2 [22].

However, the annihilation of oxygen vacancies is not proven so far and that is actually one subject of the present work. From reaction (2) one can predict that the electrode resistance will increase when the electrodes are exposed to water vapor, as a result of competing for oxygen vacancies, which are important in the electrode reaction, between the normal electrode electrochemical

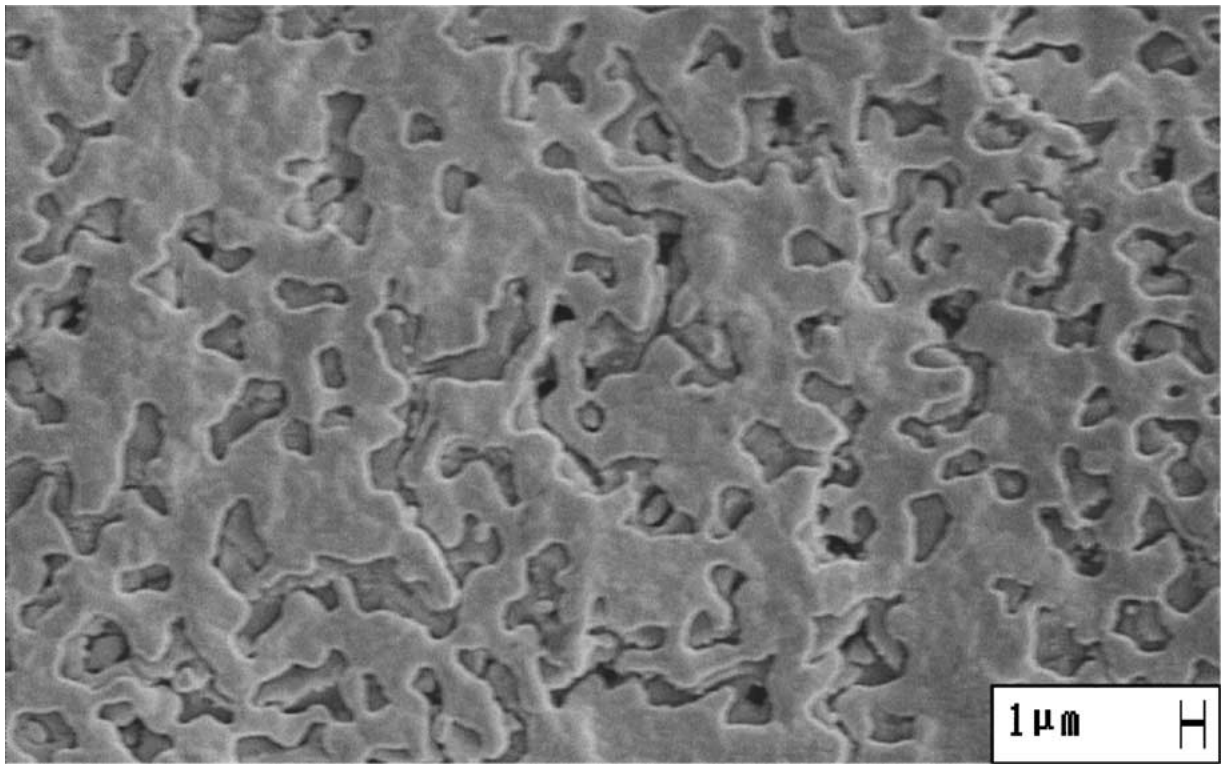

Figure 3 Typical scanning electron micrograph of porous silver electrode. The pores ensure the contact of the pellet surface with water vapor.

reaction and the degradation reaction. This point is also examined in the present work.

2. Experimental

3 mol% Y_2O_3 and 8 mol% Y_2O_3 doped ZrO_2 solid solution powders purchased from TOSOH-ZIRCONIA (Tokyo, Japan) were used. The powders were hydrostatically pressed into pellets at 200 MPa, then sintered at 1650 °C in air for 5 h. After sintering, the pellets with 3 mol% Y_2O_3 were confirmed to be tetragonal, and the pellets with 8 mol% Y_2O_3 to be cubic. The sintered pellets are 9.0 mm in diameter and 3.0 mm in thickness. Silver paint was used for electroding. The paint was applied to both surfaces of the pellets and fired at 600 °C for 1 h; porous electrodes thus resulted (Fig. 3).

Due to the large number of oxygen vacancies in the lattice, tetragonal ZrO_2 is also a good oxygen ion conductor. The variation of the oxygen vacancy concentration during the degradation, as suggested in the new mechanism, will surely change the ionic conductivity, which can be conveniently studied by impedance spectroscopy. A pellet with 3 mol% Y_2O_3 was annealed at 252 °C in water vapor for 29 h. The impedance spectrum of the pellet during annealing was measured *in situ* and every hour in a frequency range of 5 to 1 MHz with a Solartron 1260 Frequency Response Analyzer.

The electrode resistance can also be measured by impedance spectroscopy. For the sake of avoiding the complexity resulting from the phase transformation of tetragonal ZrO_2, the measurements of the electrode resistances were carried out for cubic ZrO_2. A pellet with 8 mol% Y_2O_3 was first annealed in pure oxygen at 252 °C for 1 day to ensure that the electrodes reached equilibrium with the atmosphere, then mixture of oxygen and water vapor was introduced. The estimated vapor pressure is about 2.6×10^3 Pa. The pellet was annealed in the mixture for 34 h. Immediately after that the temperature became stable at 252 °C again, the measurement of the impedance spectrum was started. The impedance spectrum was similarly measured but in a frequency range of 10^{-2} to 1 MHz in order to cover the electrode impedance. The bulk, the grain boundary and the electrode contribution to the impedence were separated by fitting the spectra with the program ZView™ (Version 2.1b, Scribner Associates, Inc.).

After annealing, the pellet with 3 mol% Y_2O_3 was subjected to X-ray diffraction (XRD) analyses with a diffractometer (type PW1710-SERIE) to detect the phase transformation caused by the annealing. The microstructures of the electrode and the fracture surfaces of the annealed pellet were observed by scanning electron microscope (SEM) (type STEREOSCAN 420).

3. Results and discussion

Typical impedance spectra of the pellet with 3 mol% Y_2O_3 at various annealing stages and the equivalent circuit for the spectra are given in Fig. 4. The change of the spectrum with annealing time is very obvious, demonstrating that impedance spectroscopy is an effective technique to monitor the degradation process. During annealing, the pellet cracked, which is reflected by the drastic change of the spectrum after 23 hours.

The sample holder helped to hold the cracked parts together during the measurement, but after removing the pellet from the holder, it fell apart. The geometrical feature of the cracked pellet is shown in Fig. 5. After annealing, the original tetragonal phase transformed into monoclinic one (Fig. 6). The cracks occurred

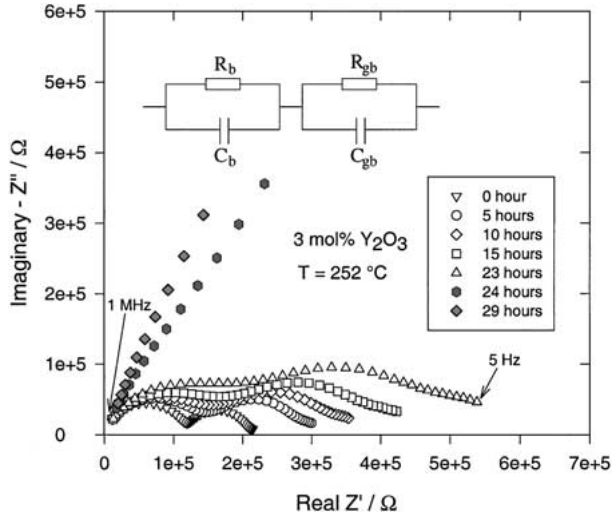

Figure 4 Impedance spectra at different annealing stages and equivalent circuit for 3 mol% Y_2O_3 doped ZrO_2.

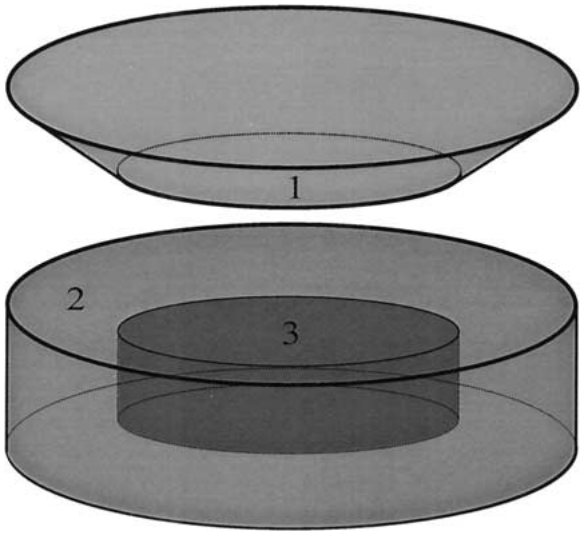

Figure 5 Schematic representation of the geometrical feature of cracked 3 mol% Y_2O_3 doped ZrO_2 pellet after annealing. The X-ray diffraction patterns of the regions 1, 2 and 3 are given in Fig. 6, while the corresponding microstructures are given in Figs 7 and 8.

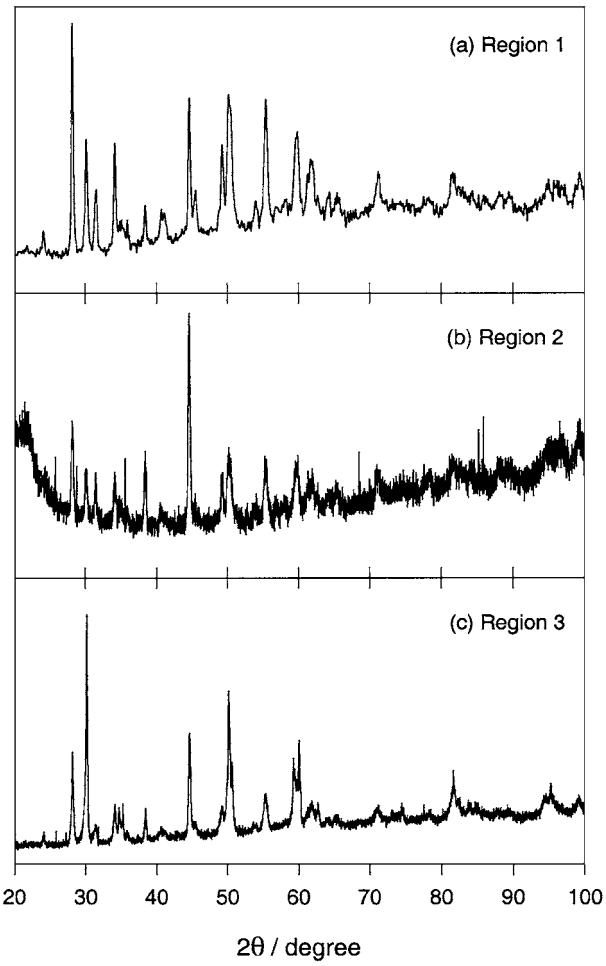

Figure 6 X-ray diffraction patterns of different regions: (a) region 1, (b) region 2 and (c) region 3. Because the region 2 is not flat, the pattern of this region is not very good. In the three regions, only monoclinic phase was detected.

intergranularly, which is obvious from Figs 7 and 8. The intergranular cracking indicates that the degradation propagated along the grain boundaries.

Fig. 9 shows the bulk and the grain boundary resistivity variation of the pellet with 3 mol% Y_2O_3 with annealing time before cracking. The resistivities were computed via $\rho = R\frac{A}{L}$, from the resistance R and the cross section area/thickness ratio A/L of the pellet. As $\rho = \frac{1}{2[V_O^{\bullet\bullet}]uF}$, with $[V_O^{\bullet\bullet}]$ being the oxygen vacancy concentration, u the mobility of the oxygen vacancy and F the Faraday constant, the variation of the resistivities directly reflects the change of the oxygen vacancy concentration. The increasing resistivities shown in Fig. 9 demonstrate that the oxygen vacancy concentrations in the bulk and at the grain boundaries were continuously decreasing during annealing, which must result from annihilating oxygen vacancies by OH^- ions. After annealing for only 1 h, the bulk resistivity jumped to a higher level, this may be due to the incorporation of OH^- ions into the surface layers and thus the annihilation of the oxygen vacancies there, further incorporation of OH^- ions was controlled by the OH^- bulk diffusion which is a lot slower than the surface process, therefore, the bulk resistivity increased only slowly but steadily in the later annealing stage. But at the experimental temperature (252 °C), the grain boundary diffusion rate is still appreciable. The grain boundary diffusion of OH^- ions annihilated the oxygen vacancies at the grain boundaries, thus increasing the grain boundary resistivity, however, at a slope much larger than that of the bulk resistivity.

A grain boundary of an oxide consists of one grain boundary core and two adjacent space charge layers [28]. Therefore, the grain boundary thickness $\delta_{gb} = \delta_{sc} + \delta_{core}$, δ_{sc} and δ_{core} are the thicknesses of the space charge layer and the grain boundary core, respectively. According to the brick layer model, the grain boundary thickness of ZrO_2 follows [29]

$$\delta_{gb} = \varepsilon_0 \varepsilon_{gb} \frac{d_g A}{C_{gb} L}, \tag{4}$$

where d_g is the average grain size, $\varepsilon_0\varepsilon_{gb}$ the dielectric constant of the grain boundary, C_{gb} the grain boundary capacitance. $d_g \approx 1.6\ \mu$m, ε_{gb} can be approximated to the dielectric constant of the bulk ε_{bulk} ($\sim 55 \pm 5$)

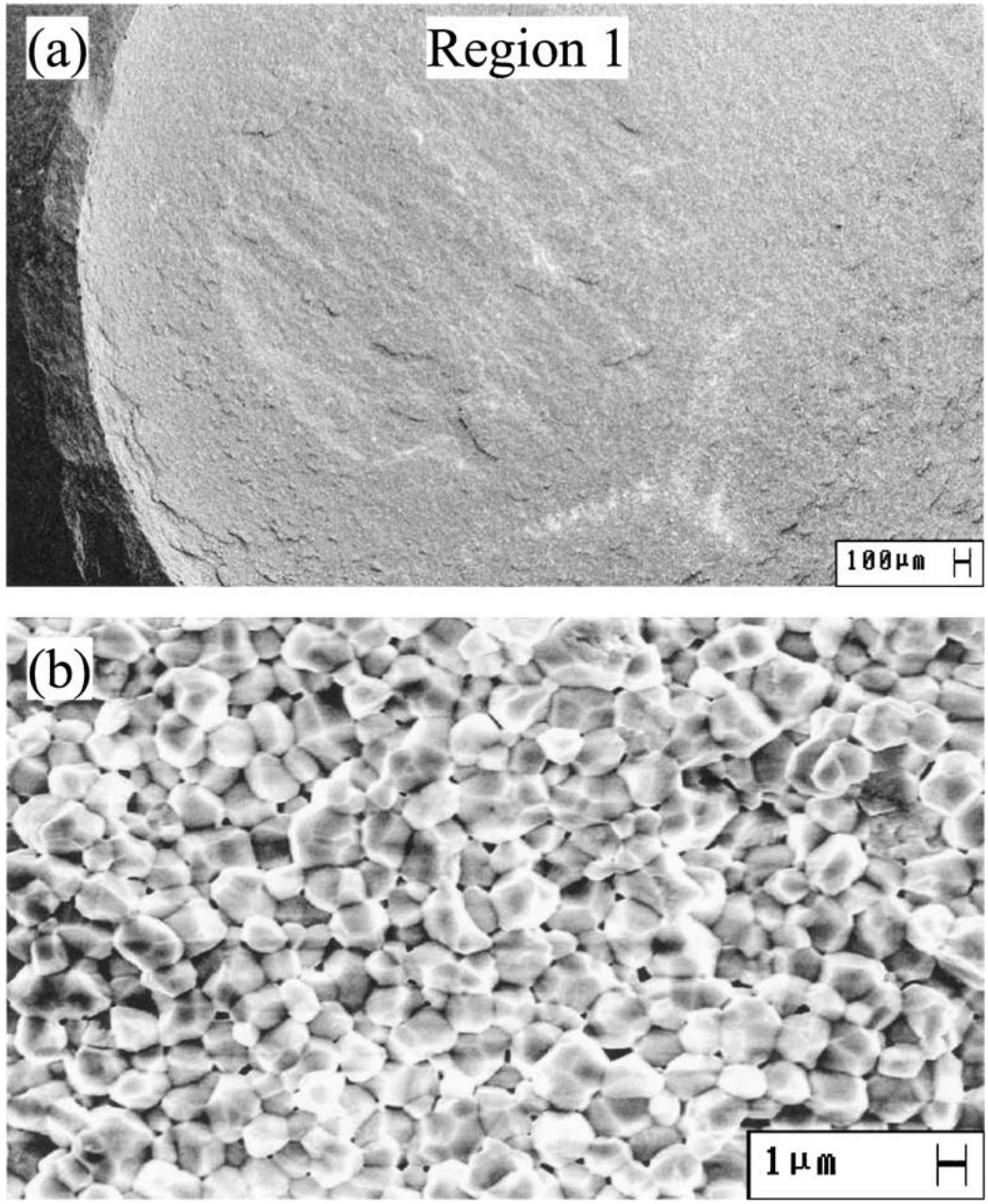

Figure 7 Scanning electron micrograghs of region 1: (a) low magnification image and (b) high magnification image. It can be seen from Fig. 7(b) that the cracks occurred intergranularly.

[30, 31], the values of C_{gb} can be derived from fitting the impedance spectra, which are given in Fig. 10. The grain boundary thickness thus calculated are also given in Fig. 10. As shown in this figure, the grain boundary thickness steadily increases with increasing annealing time.

The grain boundaries of doped ZrO_2 have been intensively studied by the author [27, 30–37], and a grain boundary defect structure model [34–37] was proposed, in which oxygen vacancy depletion and solute enrichment in the space charge layers were suggested. The core thickness of ZrO_2 was estimated to be about 0.8 nm [38], determined by geometrical factors, being thus constant during annealing. The thickness of the space charge layer is just that of the oxygen vacancy depletion layer. The steadily increasing grain boundary thickness demonstrates that the oxygen vacancy depletion layer was extending during annealing, which most possibly results from annihilating the oxygen vacancies at the grain boundaries by OH^- ions.

A typical impedance spectrum of the pellet with 8 mol% Y_2O_3 while annealed in the mixture of oxygen and water vapor is given in Fig. 11. As shown in this figure, the frequency range selected is enough to cover the electrode impedance. The electrode resistances obtained from fitting the spectra are presented in Fig. 12. In spite of the scattering of the resistance values, the overall tendency is still clear, i.e. the electrode resistance increases with increasing annealing time.

The electrode resistance reflects the limited rate of the electrochemical reaction at electrodes. For theoretically reversible electrodes, the electrode resistance is zero; but for normal (semi-blocking) electrodes, e.g. the silver electrodes on ZrO_2 in the present work, the electrode resistance is not zero. The more difficult the electrode electrochemical reaction is, the larger the

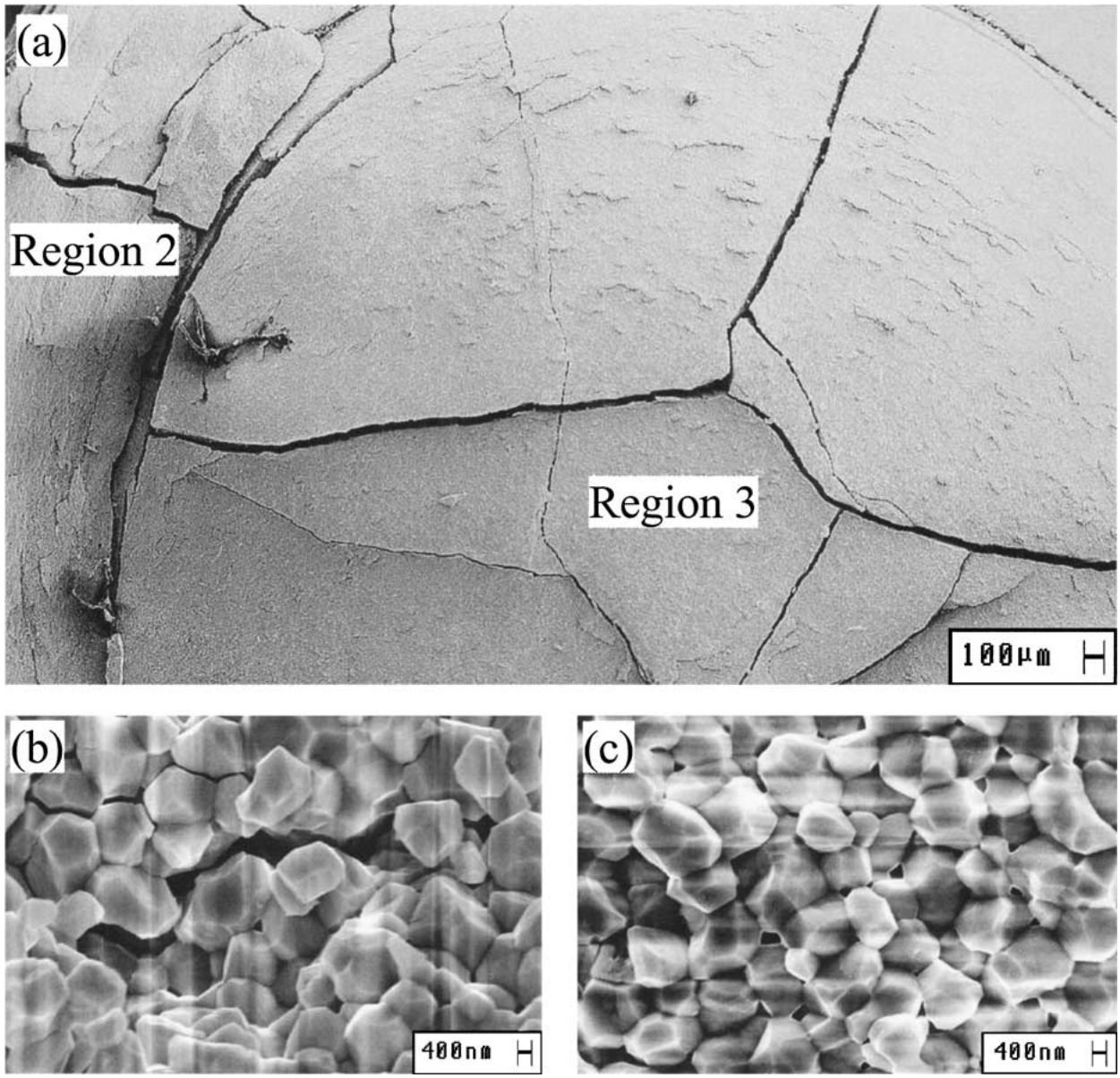

Figure 8 Scanning electron micrograghs of regions 2 and 3: (a) low magnification image of regions 2 and 3, (b) high magnification image of region 2 and (c) high magnification image of region 3. It can be seen from Figs 8(b) and (c) that the cracks occurred intergranularly. Some micro-cracks along the grain boundaries can also be observed from Fig. 8(b).

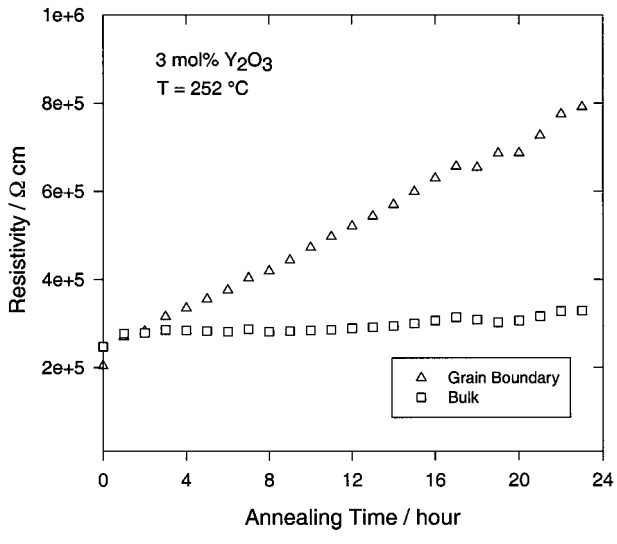

Figure 9 Resistivity vs annealing time for 3 mol% Y_2O_3 doped ZrO_2.

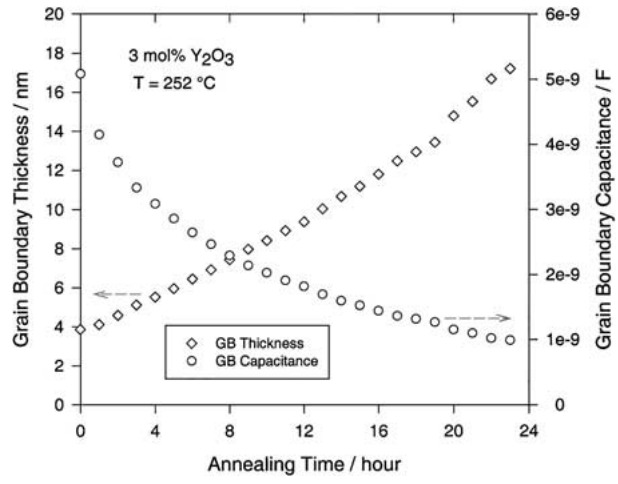

Figure 10 Grain boundary thickness and grain boundary capacitance vs annealing time for 3 mol% Y_2O_3 doped ZrO_2.

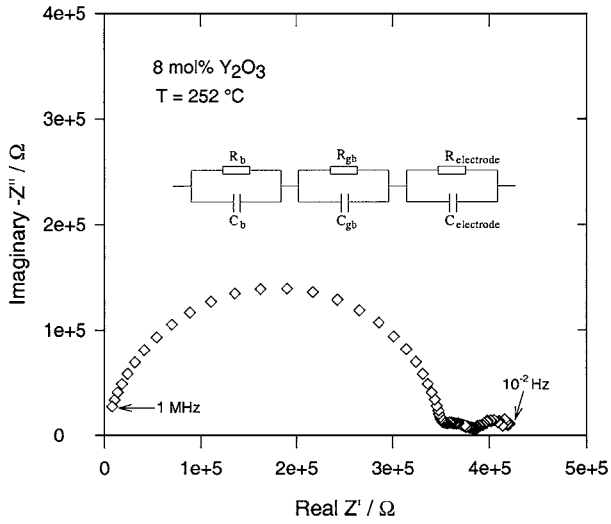

Figure 11 Typical impedance spectrum of 8 mol% Y_2O_3 doped ZrO_2 pellet in the mixture of oxygen and water vapor and equivalent circuit.

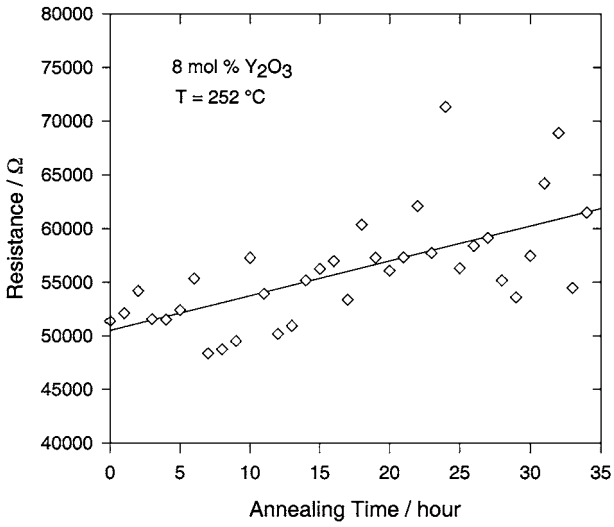

Figure 12 Electrode resistance vs annealing time for 8 mol% Y_2O_3 doped ZrO_2.

electrode resistance is. The overall electrode reaction is [39, 40]

$$\frac{1}{2}O_2(g) + 2e' + V_O^{\bullet\bullet} = O_O^x \qquad (5)$$

Oxygen gas under not extremely high partial pressure usually decreases the electrode resistance. While the silver electrodes of the present work were being annealed in pure oxygen, the electrode resistance was continuously decreasing during the first few hour of annealing, and finally reached a steady state. Therefore, the oxygen gas in the mixture of oxygen and water vapor should not be the cause for the increasing resistance shown in Fig. 12. However, reaction (2) can compete with reaction (5) for oxygen vacancies, making reaction (5) more difficult, the electrode resistance thus increased. More detailed analysis of the electrode reaction kinetics is beyond the scope of this work.

4. Conclusion

(1) Impedance spectroscopy is an effective technique to monitor the hydrothermal degradation of tetragonal ZrO_2.

(2) The annihilation of oxygen vacancies in the bulk and at the grain boundaries, and the predicted increasing electrode resistance were proven, presenting crucial supports to the degradation mechanism [20–23] previously proposed by the author.

Acknowledgement

Financial support from the Visiting Scholar Foundation of Key Lab. in University is acknowledged.

References

1. K. KOBAYASHI, H. KUWAJIMA and T. MASAKI, *Solid State Ionics* **3/4** (1981) 489.
2. T. SATO and M. SHIMADA, *J. Amer. Ceram. Soc.* **67** (1984) C-212.
3. K. TSUKAMA and M. SHIMADA, *J. Mater. Sci. Lett.* **4** (1985) 857.
4. T. SATO and M. SHIMADA, *J. Amer. Ceram. Soc.* **68** (1985) 356.
5. Y. MURASE and E. KATO, *ibid.* **66** (1983) 196.
6. *Idem.*, *Ber. Dtsch. Keram. Ges.* **57** (1980) 86.
7. T. SATO, S. OHTAKI, T. ENDO and M. SCHIMADA, *J. Amer. Ceram. Soc.* **68** (1985) C-320.
8. J.-F. LI, R. WATANABE, B.-P. ZHANG, K. ASAMI and K. H. HASHIMOTO, *J. Am. Ceram. Soc.* **79** (1996) 3109.
9. T. T. LEPISTÖ, P. V. LINTULA and T. A. MÄNTYLÄ, *Ceram. Eng. Sci. Proc.* **9** (1988) 1517.
10. F. F. LANGE, G. L. DUNLOP and B. I. DAVIS, *J. Amer. Ceram. Soc.* **69** (1986) 237.
11. T. SATO, S. OHTASHI and M. SHIMADA, *J. Mater. Sci.* **20** (1985) 1466.
12. J.-F. LI and R. WATANABE, *Mater. Transactions JIM* **37** (1996) 1171.
13. M. YOSHIMURA, T. NOMA, K. KAWABATA and S. SOMIYA, *J. Mater. Sci. Lett.* **6** (1987) 465.
14. M. YOSHIMURA, *Am. Ceram. Soc. Bull.* **67** (1988) 1950.
15. M. T. HERNANDEZ, J. R. JURADO and P. DURAN, *J. Amer. Ceram. Soc.* **74** (1991) 1254.
16. T. SATO and M. SHIMADA, *Am. Ceram. Soc. Bull.* **64** (1985) 1382.
17. T. SATO, T. ENDO, M. SHIMADA, T. MITSUDOME and N. OTABE, *J. Mater. Sci.* **26** (1991) 1346.
18. M. HIRANO, *Br. Ceram. Trans. J.* **91** (1992) 139.
19. M. YOSHIMURA, T. HIUGA and S. SOMIYA, *J. Amer. Ceram. Soc.* **69** (1986) 583.
20. X. GUO, *Solid State Ionics* **112** (1998) 113.
21. *Idem.*, *J. Phys. Chem. Solids* **60** (1999) 539.
22. *Idem.*, *Phys. Stat. Sol. (a)* **117** (2000) 191.
23. *Idem.*, *Adv. Eng. Mater.* **2** (2000) 604.
24. J. LIVAGE, K. DOI and C. MAZIERES, *J. Amer. Ceram. Soc.* **51** (1968) 349.
25. P. KOUNTOUROS and G. PETZOW, in "Science and Technology of Zirconia V," edited by S. P. S. Badwal, M. J. Bannister and R. H. J. Hannink (Technomic, Lancaster, Basel, 1993), p. 30.
26. K. D. KREUER, *Solid State Ionics* **125** (1999) 285.
27. X. GUO, *Comput. Mater. Sci.* **20** (2001) 168.
28. J. MAIER, *Ber. Bunsenges. Phys. Chem.* **90** (1986) 26.
29. T. VAN DIJK and A. J. BURGGRAAF, *Phys. Stat. Sol. (a)* **63** (1981) 229.
30. X. GUO and J. MAIER, *J. Electrochem. Soc.* **148** (2001) E121.
31. X. GUO, *Phys. Stat. Sol. (a)* **183** (2001) 261.
32. X. GUO and R.-Z. YUAN, *J. Mater. Sci.* **30** (1995) 923.
33. *Idem.*, *Solid State Ionics* **80** (1995) 159.
34. X. GUO, *ibid.* **81** (1995) 235.

35. *Idem.*, *J. Eur. Ceram. Soc.* **16** (1996) 575.
36. *Idem.*, *Solid State Ionics* **96** (1997) 247.
37. *Idem.*, *ibid*, **99** (1997) 137.
38. S. P. S. BADWAL and J. DRENNAN, *J. Mater. Sci.* **22** (1987) 3231.
39. M. KLEITZ, *Solid State Ionics* **3/4** (1981) 513.
40. A. MITTERDORFER and L. J. GAUCKLER, *ibid.* **117** (1999) 187.

Received 26 April 2000
and accepted 21 February 2001